Available online at www.easdprocedia.org
EASD Procedia EURODYN (2020) 3995-4006

EASD Procedia

EURODYN 2020
XI International Conference on Structural Dynamics
M. Papadrakakis, M. Fragiadakis, C. Papadimitriou (eds.)
Athens, Greece, 23–26 November 2020

EFFECT OF THE JOINT STRENGTH ON THE PERFORMANCE OF ORDINARY MOMENT-RESISTING FRAMES UNDER A PROGRESSIVE COLLAPSE SITUATION

Mohammad Ali Mahdavipour[1], Dmitry Vysochinskiy[1]

[1] Department of Engineering Sciences, University of Agder
Jon Lilletuns vei 9, 4879 Grimstad, Norway
e-mail: {ali.mahdavipour, dmitry.vysochinskiy} @uia.no

Keywords: Progressive collapse, Panelzone, Column removal, Ductile fracture.

Abstract. *In standard design procedures of steel structures, buildings are usually designed for gravity and seismic load rather than a progressive collapse situation. When a structure is located in a low seismic zone, the codes have dictated fewer requirements regarding the beam-to-column strength ratio and the panelzone strength. In this study, a frame subassembly from an 8-story ordinary steel moment-resisting structure with different strength of exterior joints was investigated by numerical models under a column removal situation. The results revealed that although the beam-to-column strength ratio and the panelzone strength are generally less critical parameters in the seismic design of ordinary moment-resisting frames, they can have a notable effect on the fracture pattern and the capacity of the structure under a progressive collapse. Hence a special consideration about the joints strength is needed when a structure is aimed to be designed for a progressive collapse situation.*

ISSN:2311-9020
Peer-review under responsibility of the Organizing Committee of EURODYN 2020.
doi: 10.47964/1120.9327.19341

1 INTRODUCTION

Progressive collapse is known as a rapid dynamic process that usually initiates from a local failure and propagates element-by-element to a global or partial collapse of the structure [1-4]. When a column is removed within a story of a steel structure, several sequential mechanisms act against the unbalanced vertical load. At very early stages, the beams and connections are under shear actions. In a subsequent stage as vertical displacement increases, the flexural moment at the beams becomes the dominant resisting mechanism in the frame. Finally, if the connections are ductile enough to undergo large deformations and adapt to a new configuration, the catenary action will be activated as the last resisting mechanism [1-3]. Since catenary action plays the main role in the frame resistance in progressive collapse, enough ductility of steel joints is required to develop catenary forces in the beams; otherwise, the premature global collapse of a multi-story steel structure might occur.

On the other hand, the standard design procedures of steel structures have been developed mostly for other dynamic loads like seismic load rather than a progressive collapse situation. Although the design methodology for seismic load and the progressive collapse is different, the seismic details in the steel structures would influence the performance of the connections and structures under a progressive collapse situation.

Two critical parameters of the seismic design of moment-resisting frames are the beam-to-column strength ratio and the panelzone strength. The codes [5, 6] have determined a maximum level of beam-to-column strength ratio to prevent plastic hinge formation in the columns and reduce the potential of the column-sway collapse. This limit is not obligatory for low-dissipative structures (ordinary moment frames) that are usually designed in a low-seismic zone [5, 6].

So far, the progressive collapse of steel structures has been investigated in many experimental and numerical studies [3, 7-16]; however, there are a few research studies to focus on the effect of the beam-to-column strength ratio and the panelzone strength, especially in ordinary moment frames that the strong-column-weak-beam criterion is usually neglected.

Kim and Kim [17] studied moment-resisting structures with both weak and strong panelzones by using macro-scale numerical models. The results of the nonlinear dynamic analyses showed that the influence of panelzone is dependent on the location of the removed column. The panelzone deformation could be notable if an exterior joint is engaged in the progressive collapse mechanism, while when all joints are interior, the effect of the panelzone deformation on the performance of the frame is not significant. For structures designed for high seismic load, it was also indicated that the panelzone consideration had little effect on the overall performance of the structure. In contrast, the performance of low-rise structures designed only for gravity loads could significantly be affected by the deformation of the panelzones, especially at the exterior bays. It was also reported that excessive panelzone distortion decreased the ductility demand of the beams in some cases.

In a similar study, Kordbagh and Mohammadi [18] investigated special moment-resisting frames under corner and middle column removal scenarios. The results revealed that considering panelzone in the structure with I-section columns notably increased the maximum and permanent vertical displacement of the frame, especially when the removed column was an exterior one. As a general conclusion, the panelzone effect must be considered for progressive collapse evaluation of moment-resisting structures if the panelzones were designed only for minimum requirements recommended by building codes.

Most of the previous studies used macro-level models to evaluate the effect of the beam-to-column strength ratio and the panelzone strength. Such models are not able to provide details about other level phenomena like the joints fracture mode and local plastic deformations.

2 OBJECTIVE AND SCOPE

In this paper, a frame subassembly from an exterior bay of an 8-story moment-resisting structure located in a low-seismic zone was studied under a column removal situation. In such structures, the beam-to-column strength ratio limit is usually ignored due to low seismic hazard. Therefore, two configurations of the selected subassembly with different beam-to-column strength ratios (and different panelzone strength) were investigated by nonlinear finite element simulations. A calibrated plasticity model in conjunction with a ductile damage initiation criterion was used to predict the performance of the subassemblies. These two subassemblies were compared in terms of the capacity and the pattern of ductile fracture.

3 DESCRIPTION OF THE FRAME SUBASSEMBLIES

An 8-story building with a steel moment-resisting system designed for a low-seismic area (e.g., Norway) with 0.1g design ground acceleration was selected as a case study. In terms of geometry, the structure was considered with four equal bays of 5 m (see Fig. 1(a)). Also, each story was assumed to be 3m in height. Besides seismic loads, the structure was designed for 30 kN/m and 12 kN/m uniformly distributed dead and live loads, respectively. The frame was designed according to EC8 [6] for a low ductility class with a behavior factor (q) equal to 2. In this ductility class controlling the strong-column-weak-beam criterion is not obligatory. It is worth mentioning that in the design process of this frame, strength criteria were dominant in the design of the sections, and the size of the beams was constant over the height of the building. All elements were selected from S355J2 structural steel with 355 MPa nominal yield strength. Welded Unreinforced Flange-Welded web (WUF-W) connections described in Fig. 1(c) were employed as the moment-resisting connections to resist lateral seismic loads. The weld access holes with the geometry adapted from AWS D1.8, 2016 [19] was implemented in the web of the beams to provide enough space for the flange Complete Joint Penetration welds (CJPs).

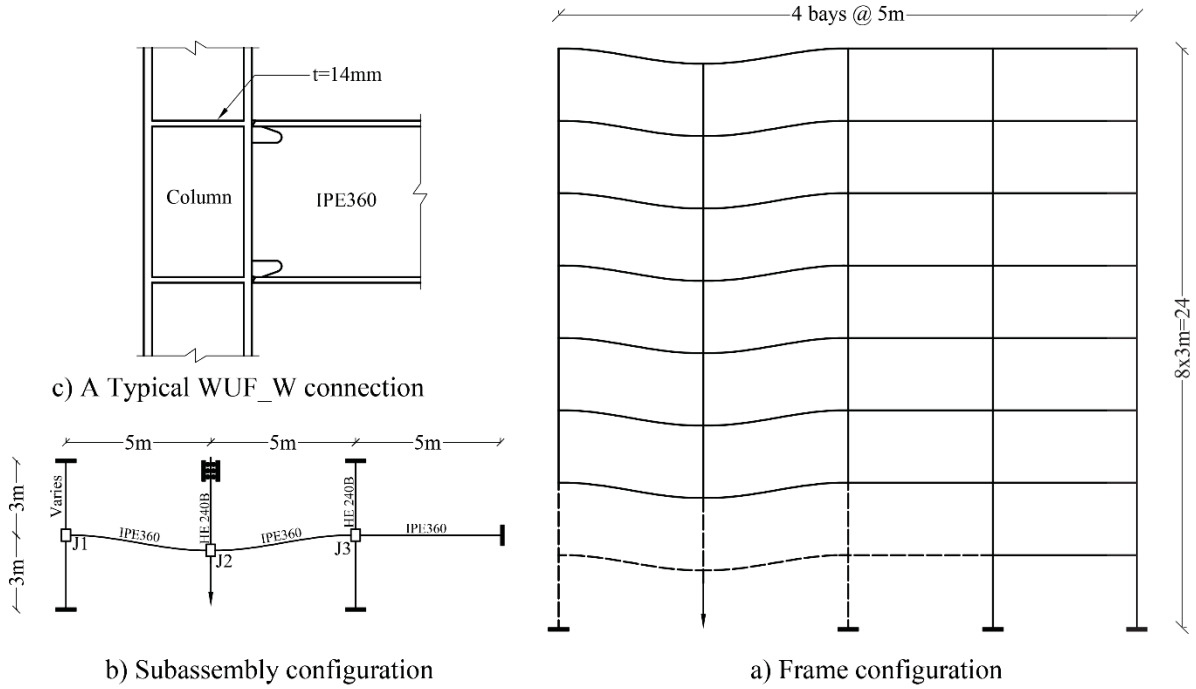

Figure 1: Configuration of a) the studied 8-story moment-resisting frame b) the subassembly c) Welded Unreinforced Flange-Welded web (WUF-W) connections.

Since analyzing the whole of the structure at the micro-level is challenging in terms of computational time and effort, a subassembly of the frame located at the first story as shown in Fig.1(b) was chosen for the finite element analyses. As it is apparent in this figure, this subassembly included three joints (J1, J2, and J3) connected by beams and columns with boundary conditions applied at the interface points between the subassembly and the rest of the frame. This subassembly was selected because the asymmetric strength of the joint J1 and J3 can also provide more detailed information regarding the effects of the beam-to-column joint strength. The previous studies also indicated that in this scenario, the panelzones have the most influence [17].

All design sections were the same in two subassemblies except the left column cross section that varies between HE180B and HE240B to study the effect of the beam-to-column strength ratio and the panelzone strength of the exterior joint. It should be noted that Subassembly-1 is from the original design of the frame that HE180B section was adequate as the left column for applied loads. On the other hand, in Subassembly-2, HE240B as the left column is a conservative design compared to the original frame.

4 NUMERICAL MODELS

4.1 Material model

Ductile fracture is known as a continuous process in which nucleation, growth, and coalescence of microvoids in ductile metals lead to form a new free surface in the material. Based on the prior studies [20-24], ductile fracture initiation is a function of equivalent plastic strain, stress triaxiality, strain rate, and Lode angle; however, the later one is less important when the structure is under tension load (positive triaxiality) [24, 25]. So far, several fracture models have been developed and utilized for predicting and evaluating the ductile fracture in steel structures. Some of these models are more complicated to be implemented (e.g., the Gurson-Tvergaard-Needleman model has over ten parameters for a single material [26]). Some other models (e.g., Johnson-Cook [20] and Bai-Wierzbicki [25]) are more appropriate for engineering applications where the uniaxial test is a standard test.

In this study, a phenomenological ductile damage model for predicting the onset of ductile fracture [27, 28] was used to investigate the fracture pattern of the studied subassemblies. In this model, it is assumed that the equivalent plastic strain at the onset of damage (ε_D^{pl}), is a function of stress triaxiality and strain rate [27]:

$$\varepsilon_D^{pl}(\eta, \dot{\varepsilon}^{pl}) \tag{1}$$

Where $\eta = {}^{\sigma_m}/_{\sigma_{eq}}$ is the stress triaxiality, σ_m is hydrostatic pressure and σ_{eq} is Mises equivalent stress. $\dot{\varepsilon}^{pl}$ also denotes the strain rate. Based on this definition, the damage variable can be defined as follows [7]:

$$D = \int \frac{d\varepsilon^{pl}}{\varepsilon_D^{pl}(\eta, \dot{\varepsilon}^{pl})} \tag{2}$$

This damage variable is an incremental state variable that increases monotonically with plastic deformations (ε^{pl}) to reach D=1 which indicates the fracture initiation. To use this model, a fracture strain curve in the space of ε^{pl}-η is needed. This curve was obtained by performing uniaxial tests under different triaxiality states for steel grade S355J2, as shown in Fig. 2. The described ductile fracture criterion was used in conjunction with the Mises plasticity and a linear isotropic hardening rule as the material model. To calibrate the stress-strain behavior of the

S355J2 material, five round smooth samples were tested under the uniaxial tensile test. Fig.3 shows the geometry of the samples.

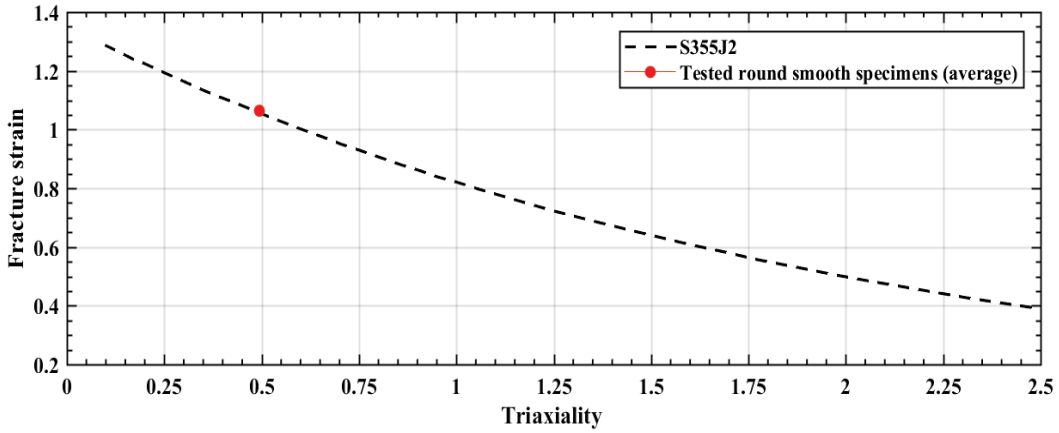

Figure 2: Fracture strain curve for S355J2 at different triaxiality.The curve adapted from [29].

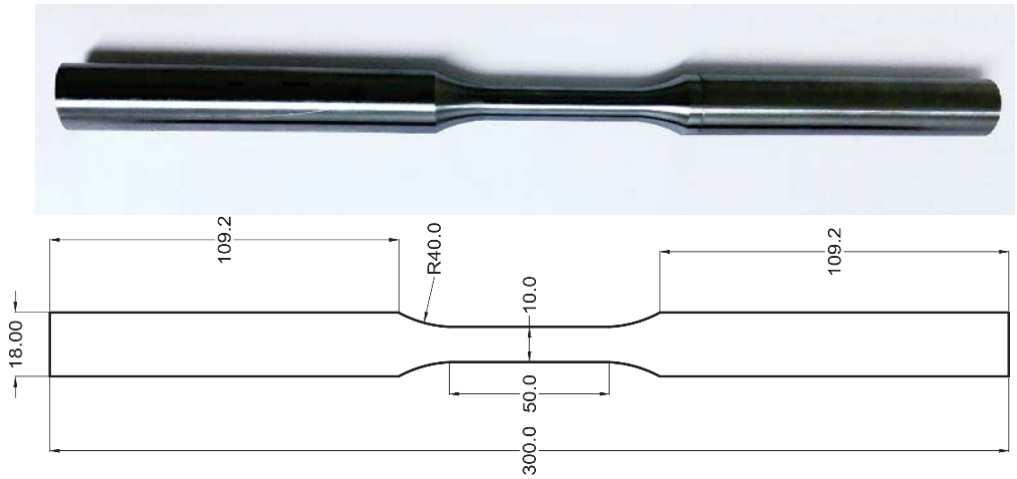

Figure 3: The geometry of round smooth tensile specimens.

All specimens were taken from a flat plate with 25mm thickness in the rolling direction. It should be noted that the effect of the strain rate was outside of the scope so that all tests were conducted at a strain rate of 0.002 mm/mm/s.

A 50mm axial extensometer and a digital image correlation system (DIC) were used to measure the elongation of the gage length. Using DIC can provide the fracture strain of each sample precisely. For example, as shown in Fig. 4, the fracture strain was 1.047 and 1.075 in sample MU1 and MU4, respectively. The engineering stress-strain curves for all tested samples are illustrated in Fig. 5.

To calibrate the ductile damage model an average fracture strain of all five samples ($\bar{\varepsilon}_f = 1.064$) was used. The point corresponding to the average fracture strain and triaxiality of the samples is plotted in Fig. 2 to validate the curve at least at one point. Since the stress triaxiality is varying after the necking of the samples, an average value was obtained ($\bar{\eta} = 0.49$) from the numerical simulation. Fig. 2 indicates a good agreement between the curve and experimental results for round smooth bar samples (plotted by a red circle).

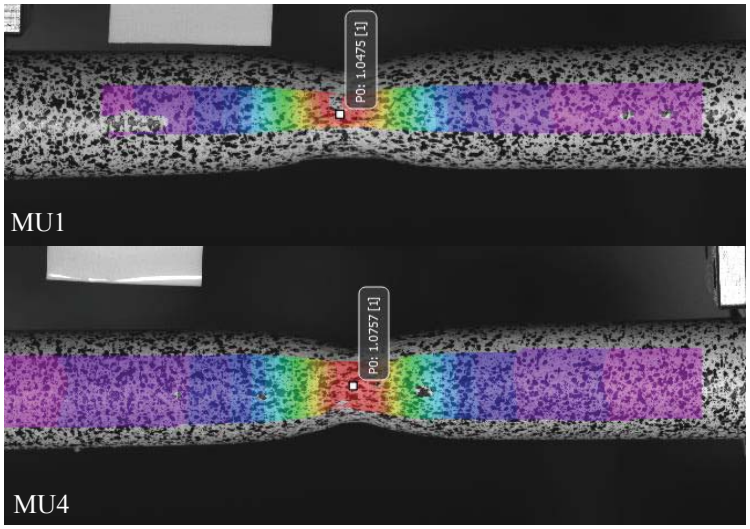

Figure 4: Fracture strain of samples MU1 and MU4 extracted from DIC.

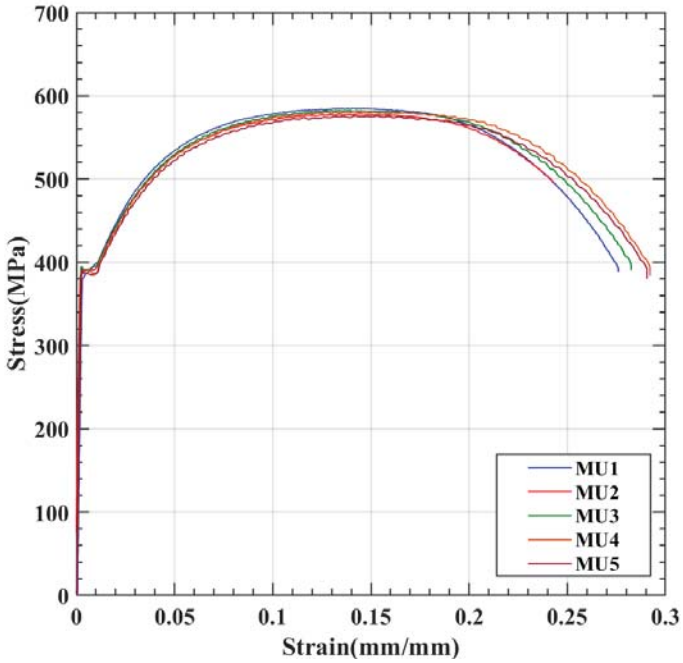

Figure 5: Engineering stress-strain curves for tested round smooth bar samples.

To use the test data in the material plasticity model, true stress-strain curves are required. Before the necking that the uniaxial state is governed, the true strain and stress can be obtained as follows:

$$\varepsilon_t = \ln(\varepsilon_e + 1)$$
$$\sigma_t = (1 + \varepsilon_e)\sigma_e \tag{3}$$

Where ε_t and σ_t are true strain and stress respectively, while ε_e and σ_e denote engineering values.

After necking, these relations are invalid due to stress triaxiality and strain localization. Therefore, a linear transition was assumed between the ultimate and the fracture point. The fracture strain could be obtained by DIC; however, the equivalent true fracture stress also

should be calculated to consider the triaxial stress state. Bridgman proposed an approximate conversion from a triaxial stress state into an equivalent stress σ_{eff} by using the geometry of the samples as follows [30]:

$$\sigma_{eff} = \frac{\sigma_t}{(1 + \frac{4R}{D}) \times ln(1 + \frac{D}{4R})} \tag{4}$$

Where D is the diameter of the sample, and R is the radius of curvature at the fracture point. These two parameters can be measured at the fracture point by image processing (e.g., See Fig. 6 for sample MU1).

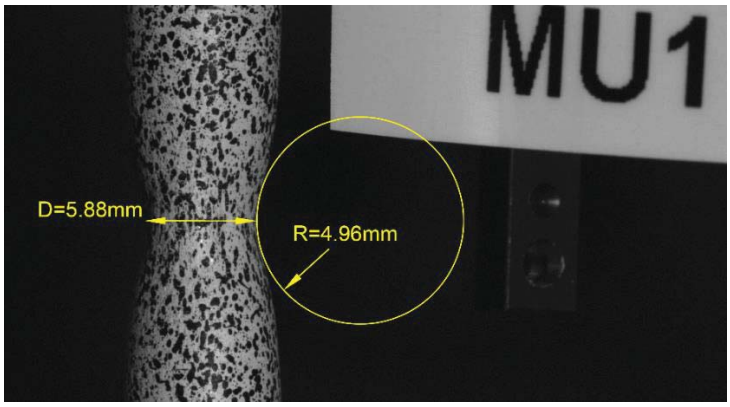

Figure 6: The diameter of the sample and the radius of curvature at the fracture point for sample MU1.

The calibrated material plasticity and damage model verified by numerical models. For instance, Fig. 7 compares the experimental and numerical force-displacement curves for the MU1 specimen. As this figure shows, there is a good agreement between numerical and experimental curves.

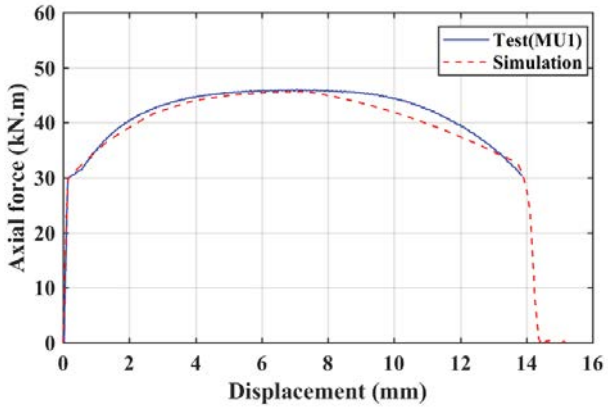

Figure 7: Ductile damage model verification for sample MU1.

4.2 Finite element models of the subassemblies

To predict the ductile fracture of two pre-described subassemblies, nonlinear finite element models were created in Abaqus/CAE. The explicit solver was employed due to its efficiency in conducting and converging extreme nonlinear behavior, particularly when a fracture and material separation are simulated. The simulations were implemented as a quasi-static to find the

capacity of the subassemblies and track the fracture behavior of the components under incremental displacement imposed at the point of the removed column.

For all nonlinear parts around the beam-to-column joints, the eight-node solid brick elements with reduced integration points (C3D8R) with a fine mesh were applied for the discretization of the models (see Fig. 8). These fine-meshed domains were assumed to have a length at least equal to the depth of beam or column that is known as the most probable place for plastic hinges formation. In these areas, the thickness of beams flanges and webs divided into at least four layers of element.

On the other hand, the middle parts of the beams and columns were modeled by a coarse mesh to reduce the time of analyses. To make an appropriate transition between the fine-meshed and the coarse-meshed areas a combination of C3D8R and six-node wedge element (C3D6) was used as shown in Fig. 8. It is worth mentioning that in numerical models, the properties of the welds were ignored.

An incremental displacement was applied to the removed column at joint J2, and the boundary conditions were defined as shown in Fig. 1(b). Also, it was supposed that beams flanges and columns at the joint level are laterally braced due to the slab system and secondary beams.

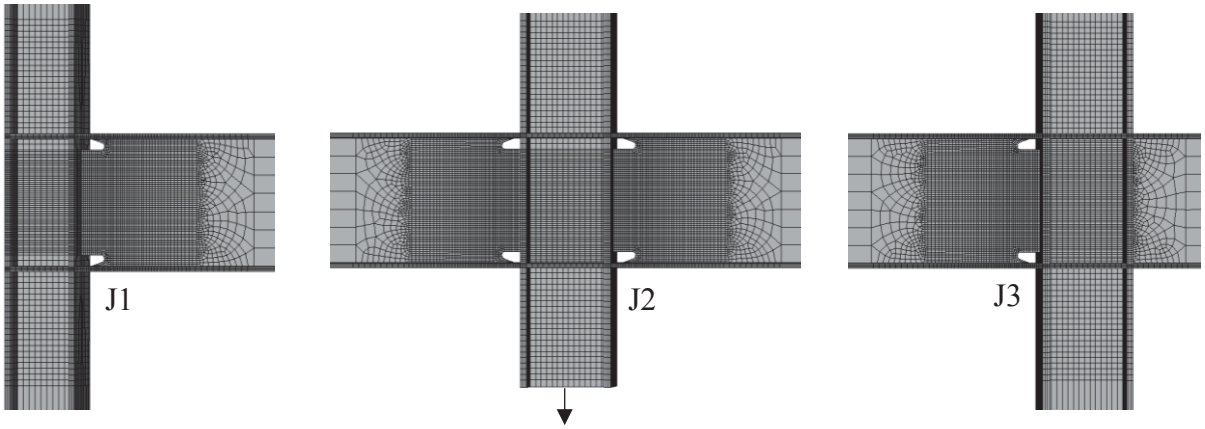

Figure 8: Finite element discretization of subassemblies with a fine mesh around the joints.

5 RESULTS

Fig. 9 compares the force-vertical displacement of two described subassemblies. Comparing of the subassemblies can be done in different aspects and parameters. In terms of yielding strength, both subassemblies provided approximately similar global yielding strength; however, due to the panelzone distortion in the Subassembly-1 with HE180B column, the panelzone in J1 was the first component that experienced plastic deformations, while the beam in this joint had a limited plastic strain even at the last step of the analysis. Moreover, this panelzone distortion imposed the maximum equivalent plastic strain (PEEQ) in the upper column of the joint J1. Forming plastic hinge and excessive lateral deformation of the column can increase the potential of post-yield buckling of the column under axial loads. In contrast, in the other subassembly (with HE240B column) the panelzone yielded after some plastification in the beam so that in the last step of the analysis, the maximum PEEQ occurred in the beam area while the upper column exhibited a low amount of plastic deformations.

Before any fracture initiation in the subassemblies, the Subassembly-2 with stronger joint J1 provided significantly more vertical strength. For example, in the vertical displacement of 877mm that is corresponding to the onset of fracture in the bottom flange of the joint J2 in the

Subassembly-2, the vertical strength of this subassembly was about 44% more than Subassembly-1.

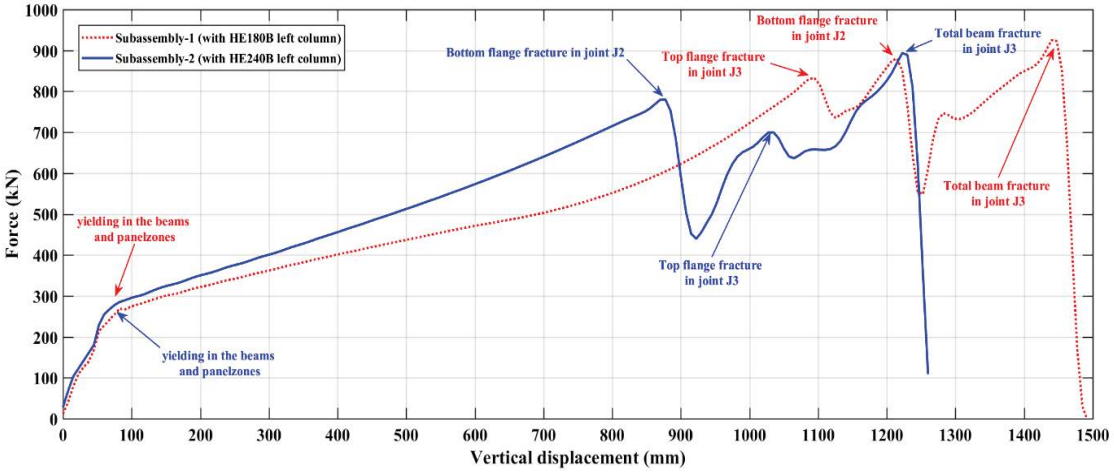

Figure 9: Vertical force-displacement curves for two studied frame subassemblies.

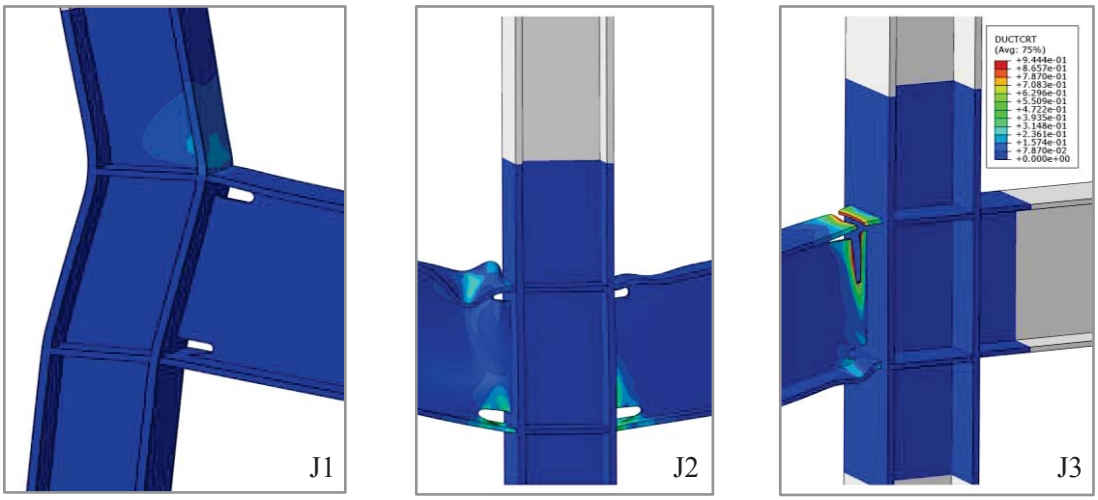

Figure 10: Distribution of ductile damage variable (D) at different joints in Subassembly-1 (ductile fracture initiated and developed firstly in J3)

In terms of ductile fracture initiation pattern, as shown in Fig.10 for the Subassembly-1, due to unbalanced stiffness and catenary action in the two sides beams, the fracture firstly initiated at the top flange of the beam in J3 joint and then developed to the web of the beam. When the right beam lost some amount of its stiffness, the fracture also initiated at the bottom flange in the other side beam in the joint J2.

On the other hand, the Subassembly-2 exhibited a vice-versa fracture initiation pattern. In other words, due to the stronger J1 joint, the stiffness and catenary action is more balanced than the Subassembly-1. As Fig.11 indicates the fracture initiated at the left beam of the joint J2. By developing the crack in the beam web and decreasing the beam stiffness, the J3 joint finally experienced the fracture at the top flange of the beam.

An interesting trend can be drawn from Fig.9 although the complete fracture of beams for both subassemblies happened in joint J3 and the cap vertical forces of both subassemblies are approximately similar, the Subassembly-1 exhibited larger vertical displacement than the Subassembly-2. This extra displacement caused by the excessive distortion of joint J1 (less stiffness) that delayed the activation of the catenary action in the beams. As a result, a weak panelzone

can significantly increase the vertical displacement demand of the frames and have to be considered in the frame analysis.

In addition, if the maximum vertical displacement demand obtained from the nonlinear dynamic analysis of the frame under similar column removal scenario was less than vertical displacement corresponding to ductile fracture initiation of subassemblies (in the capacity curves), using a simplified material model like a bilinear model can provide valid results in nonlinear dynamic analysis of the frame.

All these conclusions were made based on the assumption that welds material possesses higher toughness than base metal and the welds are without defects and significant stress and strain concentration.

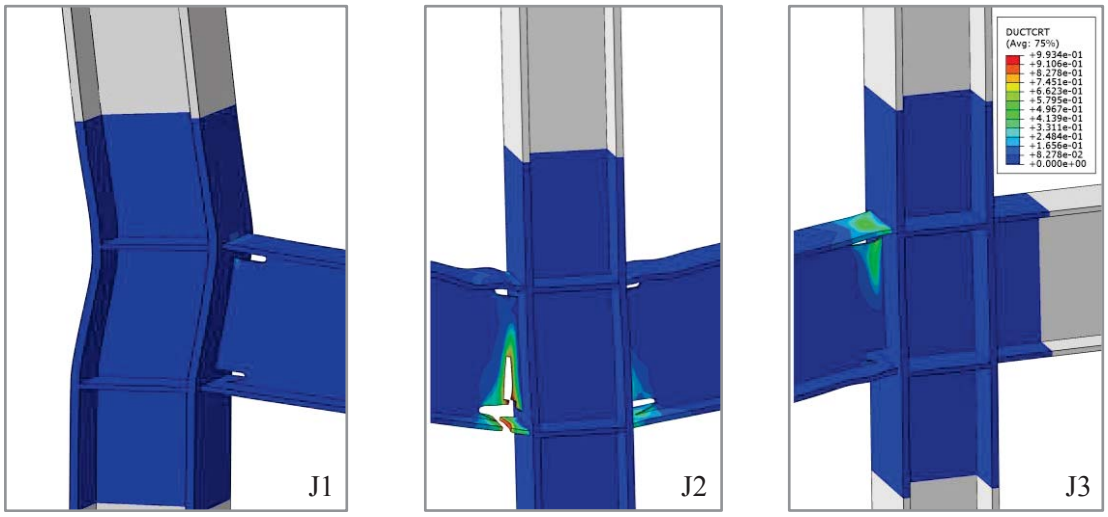

Figure 11: Distribution of ductile damage variable (D) at different joints in Subassembly-2 (ductile fracture initiated and developed firstly in J2)

6 CONCLUSIONS

A frame subassembly from an 8-story ordinary steel moment-resisting structure was studied for a column removal situation. The capacity and the fracture pattern of the subassembly obtained for different exterior joint strength. Based on the results from numerical models, the following conclusions can be drawn:

- The strength of the exterior joints in outer bays of such structures can significantly affect the fracture pattern and the capacity of the frame under a column removal situation.
- When an exterior weak joint was used, excessive plastic deformation of the panelzone led to an unbalanced state in catenary action so that the asymmetric force induced the fracture at the end of the right beam near to the interior joint. In contrast, when a stronger exterior joint was used, the rigidity of the panelzone led to make a balanced state in catenary action so that the fracture occurred at the left beam near to the middle joint that the column was removed.
- Before any fracture initiation, the vertical strength of the specimen with a stronger exterior joint showed about 44% more strength than the model with a weaker exterior joint; however, the maximum resisted vertical force for both models was approximately similar.

- In general, although the beam-to-column strength ratio and the panelzone strength usually are less critical in the standard procedure of design of moment-resisting structures in a low seismic zone, special consideration is needed when such structures are also designed for a progressive collapse situation.

REFERENCES

[1] Ellingwood BR, Smilowitz R, Dusenberry DO, Duthinh D, Lew HS, Carino NJ. Best practices for reducing the potential for progressive collapse in buildings. 2007.

[2] General Services Administration. Alternate path analysis & design guidelines for progressive collapse resistance. 2013.

[3] Sadek F, Main JA, Lew HS, Robert SD, Chiarito VP, El-Tawil S. An experimental and computational study of steel moment connections under a column removal scenario (NIST Technical Note 1669). National Institute of Standards and Technology; 2010.

[4] American Society of Civil Engineers. ASCE Standard ASCE/SEI 7-10: Minimum Design Loads and Associated Criteria for Buildings and Other Structures. Reston, Virginia2010.

[5] AISC. Seismic provisions for structural steel buildings (ANSI/AISC 341-10). Chicago(IL): American Institute of Steel Construction; 2010.

[6] European Committee for Standardization. Eurocode 8: Design of structures for earthquake resistance-part 1: general rules, seismic actions and rules for buildings (EN 1998-1). European Committee for Standardization,Brussels2004

[7] Botez M, Bredean L, Ioani A. Improving the accuracy of progressive collapse risk assessment: Efficiency and contribution of supplementary progressive collapse resisting mechanisms. Computers & Structures. 2016;174:54-65.

[8] Jiang B, Li G-Q, Usmani A. Progressive collapse mechanisms investigation of planar steel moment frames under localized fire. Journal of Constructional Steel Research. 2015;115:160-8.

[9] Jiang J, Li G-Q. Disproportionate collapse of 3D steel-framed structures exposed to various compartment fires. Journal of Constructional Steel Research. 2017;138:594-607.

[10] Khandelwal K, El-Tawil S. Collapse behavior of steel special moment resisting frame connections. Journal of Structural Engineering. 2007;133:646-55.

[11] Khandelwal K, El-Tawil S. Pushdown resistance as a measure of robustness in progressive collapse analysis. Engineering Structures. 2011;33:2653-61.

[12] Khandelwal K, El-Tawil S, Kunnath SK, Lew H. Macromodel-based simulation of progressive collapse: Steel frame structures. Journal of structural engineering. 2008;134:1070-8.

[13] Kim T, Kim J. Collapse analysis of steel moment frames with various seismic connections. Journal of Constructional Steel Research. 2009;65:1316-22.

[14] Rahnavard R, Fard FFZ, Hosseini A, Suleiman M. Nonlinear analysis on progressive collapse of tall steel composite buildings. Case studies in construction materials. 2018;8:359-79.

[15] Li L, Wang W, Teh LH, Chen Y. Effects of span-to-depth ratios on moment connection damage evolution under catenary action. Journal of Constructional Steel Research. 2017;139:18-29.

[16] Li L, Wang W, Chen Y, Lu Y. Experimental investigation of beam-to-tubular column moment connections under column removal scenario. Journal of Constructional Steel Research. 2013;88:244-55.

[17] Kim T, Kim J. Progressive collapse-resisting capacity of steel moment frames considering panel zone deformation. Advances in Structural Engineering. 2009;12:231-40.

[18] Kordbagh B, Mohammadi M. Influence of panel zone on progressive collapse resistance of steel structures. Journal of Performance of Constructed Facilities. 2018;32:04018014.

[19] American Welding Society (AWS) D1 Committee on Structural Welding. Structural welding code-seismic supplement (AWS D1.8/D1.8M:2016). MA: American Welding Society; 2016.

[20] Hancock J, Mackenzie A. On the mechanisms of ductile failure in high-strength steels subjected to multi-axial stress-states. Journal of the Mechanics and Physics of Solids. 1976;24:147-60.

[21] Johnson GR, Cook WH. Fracture characteristics of three metals subjected to various strains, strain rates, temperatures and pressures. Engineering fracture mechanics. 1985;21:31-48.

[22] McClintock FA. A criterion for ductile fracture by the growth of holes. Journal of applied mechanics. 1968;35:363-71.

[23] Rice JR, Tracey DM. On the ductile enlargement of voids in triaxial stress fields. Journal of the Mechanics and Physics of Solids. 1969;17:201-17.

[24] Bao Y, Wierzbicki T. On fracture locus in the equivalent strain and stress triaxiality space. International Journal of Mechanical Sciences. 2004;46:81-98.

[25] Bai Y, Wierzbicki T. A new model of metal plasticity and fracture with pressure and Lode dependence. International journal of plasticity. 2008;24:1071-96.

[26] Jia L-J, Ge H. Ultra-Low Cycle Fatigue Failure of Metal Structures Under Strong Earthquakes: Springer; 2018.

[27] Dassault Systèmes. Abaqus analysis user's manual. Simulia Corp. Providence, RI, USA2013.

[28] Hooputra H, Gese H, Dell H, Werner H. A comprehensive failure model for crashworthiness simulation of aluminium extrusions. International Journal of Crashworthiness. 2004;9:449-64.

[29] Hradil P, Talja A. Ductility limits of high strength steels. Research report VTT; 2016.

[30] Öchsner A. Continuum Damage and Fracture Mechanics: Springer; 2016.